

Simulation of Fracture at Different Loading Rates Using Molecular Dynamics

Juwhan Kim, Jihoon Lim & Yun Mook Lim

School of Civil & Environmental Engineering, College of Engineering, Yonsei University, Seoul(120-749), Korea

ABSTRACT: Every material changes its failure behavior under different loading rates, and this is the so-called rate dependency of materials. In particular, brittle and quasi-brittle materials show significant change of strength and strain capacity under different loading rates. Usually this phenomenon can be found experimentally, and this effect can be utilized in many engineering aspects. Thus, formulas based on experimental results have been adopted to predict material failure behavior under a given loading rate in engineering design. Most of the parameters are expressed through diagrams as functions of strain rate. Therefore, if the strain rates are assigned for a certain application of materials, the dynamic factors can be picked from the curve. The strength under the given loading rate can be defined as a factor which multiplies the strength under a quasi-static loading condition. However, this method depends on massive experimental works, and there is still a lack of understanding of fundamental behavior of the material failure characteristics.

In this paper, the fundamental failure behavior of brittle material under different loading rates is observed using a numerical simulation based on the molecular dynamics analysis. A brittle material is modeled by numerous particles with a multi-scale analysis scheme. Each particle has interactions with the other particles with Lennard-Jones potential between particles. Sub-million particles are modeled for a simulation. Numerical simulations are performed with different loading rates in a direct tensile test on specimen with a notch. The loading rates are varied over a broad range which includes the stress wave velocity of the material. The trend of the strain capacity curve and crack propagation profile can be achieved from the simulations with various loading rates. The results will provide a detailed description of failure mechanism which changes with different strain rates.

1 INTRODUCTION

Experimentally, it is reported that the fracture behavior of materials changes at different strain rates, or high loading rates. Especially in the case of brittle material such as concrete under impact loading, the effect of dynamic loading can be significant (John and Shah 1990). Characteristics of the dynamically induced fracture are, however, yet to be fully understood due to the complexity of the experiment setup and limited knowledge of controlling parameters that determine the failure mode. The difficulty of sustaining constant strain rate and the presence of wave motion in specimens often necessitates an indirect experimental method such as using a Hopkinson bar. An example of such an experiment can be found in the research of Lok et al. (Lok, Zhao, and Lu 2003). They found that the splitting strength increases significantly upon dynamic loading, and the steel fibre reinforced concrete they tested lost ductility at high strain rate.

Recently, a direct method of analysis, namely molecular dynamics (MD), has been introduced into

the engineering community to help understand such a phenomena. The method enables a direct and detailed analysis of materials under highly dynamic conditions. Unlike conventional methods such as a finite element (FE) or a finite difference (FD), MD starts from basic rules that define intermolecular force and does not require experimentally determined parameters that control material behavior. Instead, the parameters can be found from the numerical *experiments*. Normally in FE and FD, the parameters must be known as *a priori* at the time of analysis, and the quality of the simulation largely depends on the accuracy of the parameters. The molecular dynamics has been applied to the dynamic simulation of fracture to identify dynamic features such as an inter-sonic crack propagation (Gao, Huang, and Abraham 2001), polycrystalline effects (Krivtsov and Wierciogoch 2001), and dynamic instability due to hyperelasticity (Buehler and Gao 2006; Buehler, Abraham, and Gao 2003).

This research attempts to identify a change of the

failure mode and give an insight about fracture behavior under dynamic loading. Wagner et al. (Wagner, Holian, and Voter 1992) conducted a similar study to simulate material behavior at a high strain rate. However, their effort was based on a fairly small size of specimens (16000 particles used), and the specimens were placed inside periodic boundaries which did not explicitly simulate a fracture mechanism. This study presents a modernized numerical *experiment* on the same material (a Lennard-Jones(LJ) potential based material) with explicit boundary conditions and a notch, so that the result will provide a qualitative understanding of the fracture mechanism.

2 COMPOSITION OF SPECIMENS

First, the governing equation is normalized by using the pseudo-sonic speed v_s and the equilibrium separation length r_0 . The equilibrium separation length r_0 is the length where the inter-particle force derived from the LJ potential is zero. The elastic spring constant at the small deformation is then formulated by taking the slope of the displacement-force curve at r_0 . The spring constant is used to calculate v_s . The velocity in analysis is normalized as the mach number, which is the actual velocity divided by v_s , and the spatial position is transformed to the particle length q , which is the actual length divided by r_0 .

Second, the average mach number of particles in terms of v_s is calculated at the melting point. It turns out that the normalized system depends only on v_s of the target material, and once the value is known, the average mach number at the melting point is an invariant among different materials. Hence, the model renders multiscality where parameters are not tied to a specific material.

Third, the MD particles are packed in a notch configuration. The Velocities of target particles are set to a target value, which represents the temperature of the material, i.e., the mach number is calculated using a fraction of the melting point. The initial condition simulates a situation where all particles share the same velocity, which is non-physical. However, the direction of the velocity is randomized so that in the successive equilibration the velocity distribution converges to the Maxwell-Boltzmann shape while retaining the average kinetic energy. The generic configuration of the specimen is shown in Figure 1. The container is in particle dimensions of 600 by 600, and the notch extends to 50% of the height from the bottom. Extra particles are padded at the left and right sides to simulate clamps. 10 layers of particles on each side are added, and the boundary layers are displaced according to the designated strain-rate. The total number of particles is approximately 0.41 million.

Fourth, specimens are put under pre-analysis where boundaries are put at rest. In the process, the velocity distribution equilibrates and the particles move to the optimal position to achieve thermal equilibrium. This approach differs from the method proposed by

Krivtsov and Wiercigroch (2001). Krivtsov and Wiercigroch took a progressive approach where particles are shot into a container until a desired particle density is achieved. This study takes an instantaneous approach where particles are placed at a regular grid (for the purpose of the study, a hexagonal grid with spacing at r_0 is used.) with constant velocity and randomized direction. It is observed during the equilibration that the configuration generated by Krivtsov and Wiercigroch can be replicated by the instantaneous method with less computational effort.

Finally, the specimens are put under various loading rates (0.1, 0.3, 0.5, 1.0, and 5.0% of v_s) of tension to initiate crack propagation. At each time step, normalized positions of particles, along with velocity expressed in the mach number are recorded. The mach number is used to calculate the local temperature at the particle. For further processing, positions of particles are triangulated using the Delaunay tessellation, then the Voronoi cells for particles are generated using the triangulation. The area occupied by each Voronoi cell is calculated, and then a number density corresponding to the area is assigned to each particle. For visualization, the density diagram is projected onto a graphical view port (800 by 800 pixels image) with a density value byte scaled to assist identifying features. The velocity received similar treatment in that it is converted to a fraction of the melting point. The value set is then triangulated, interpolated, and projected.

3 RESULTS

Figure 2 shows results of the simulation in density snapshots. Several notes should be made about the arrangement of the figure:

- Due to the existence of wave motion, external displacements applied at the left and right boundaries take time to reach the notch placed at

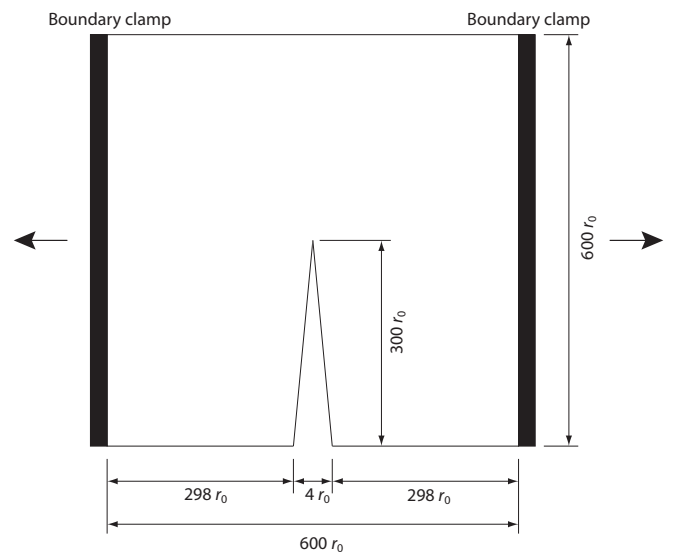


Figure 1. Configuration of the test specimen. Dimensions are in particle units, and 10 layers of boundary particles are padded on both left and right sides to simulate clamps.

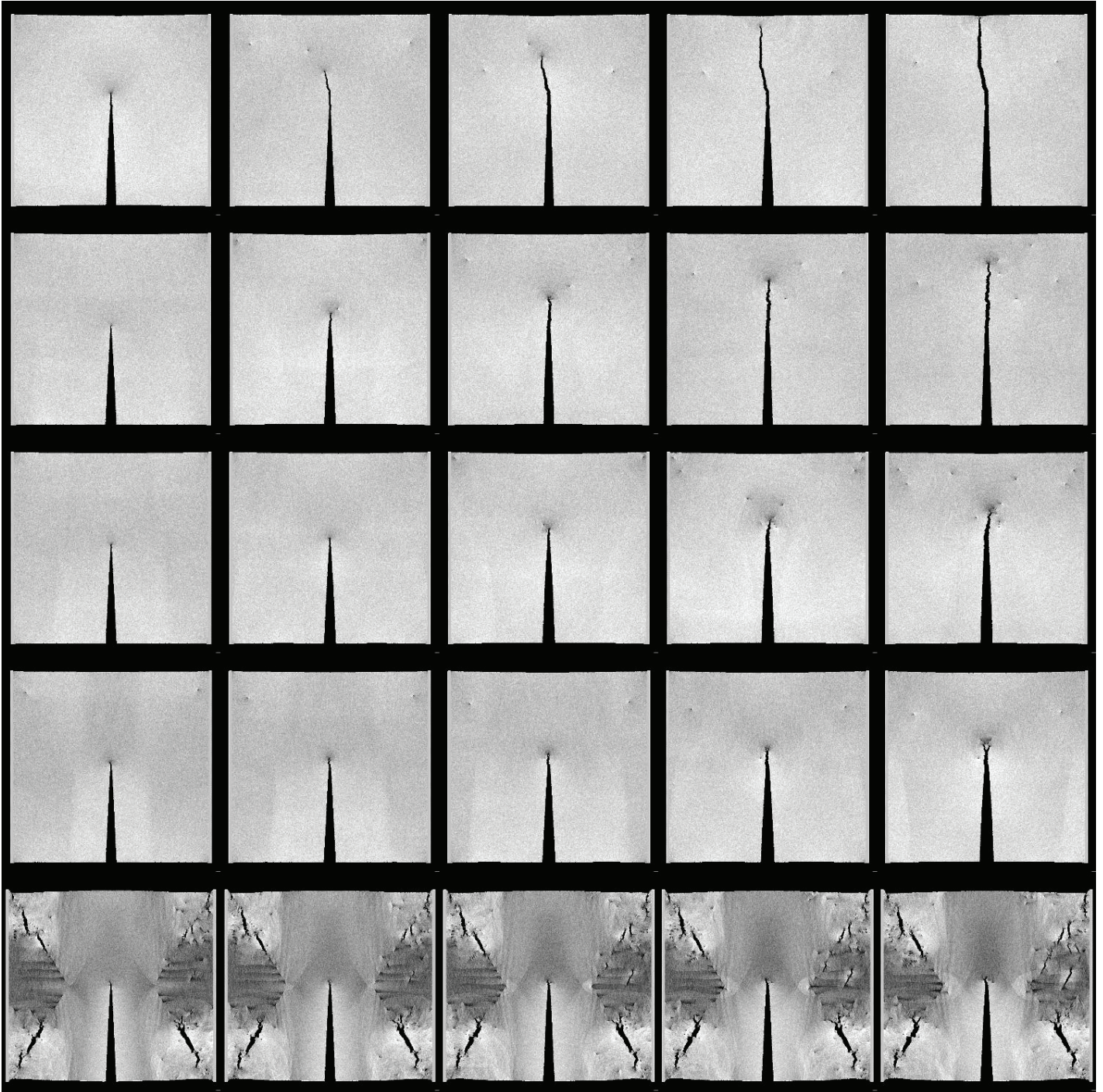


Figure 2. Crack propagation profile represented in density variation. Specimens corresponding to 5 different loading rates (0.1%, 0.3%, 0.5%, 1.0%, and 5.0% of v_s) are arranged in rows, and each column depicts a snapshot at the same global strain (0.15%, 0.3425%, 0.535%, 0.7275%, and 0.92%). Brightness of the figure is byte scaled to number density of 1.0–1.2.

the center. In other words, the notch needs time to feel the external loading. The time required for the loading wave to reach the notch t_0 is approximately $t_0 = L/(2v_s)$ where $L = 600r_0$. Hence, each simulation is offsetted by t_0 to compensate for the initial delay,

- Due to strain rate and strain variation inside the domain, the loading rate (in fraction of v_s) and the global strain ($2\Delta/L$ where Δ is the boundary displacement) are used as control parameters.
- Instead of time-based snapshots, global strain-based snapshots are arranged in columns. The arrangement visualizes the crack length versus the global strain relationship similar to the conventional stress-strain relationship. Also note that the time to achieve the same global strain is different for each case.

Crack propagation is noticeably retarded at higher loading rates. While the case of 0.1% of v_s shows an almost complete separation of the specimen at the final stage, case 0.3% shows approximately 80%, case 0.5% shows approximately 30%, and case 1.0% shows approximately 5% of crack growth. The feature can be related to the toughness of the material. It may indicate that toughness of the material increases as loading rate increases. The case shown in the last row of Figure 2 is when the loading rate is at 5% of v_s . For this case, instead of failing in fracture mode, the material failed in spallation. The shockwave generated at the boundaries did not reach the notch at the center. Instead the shockwave destroyed the near-boundary region. The spallation follow a specific pattern so that crack generation and growth follows a triangular shape. It is interesting to see that at high loading rates, the notch does not play a dominant role in determining the failure mode.

Dark regions in Figure 2 represent the lower density zone. Lower density may indicate softening of the material in that potential energy in the region tends to be depleted. The low density zone appears more protruded in higher loading rate cases. Especially in the cases of 0.5% and 1.0% of v_s , the zone appears ahead of the crack tip. This may indicate that energy consumption is more active in the higher loading cases, and a greater area becomes active in the process. The low density zone can affect direction of the crack growth (Gao, Huang, and Abraham 2001). It may also be related to the smoothness of the cracked surface. At lower loading rates, the cracked surface appears smoother than at higher rates. Not shown in the figure is the crack stoppage. In the course of analysis, it was observed that for the case of lower loading rates, crack growth initiates through a clean and smooth path, then stops, develops a rough opening, then initiates again.

Figure 3 shows the configuration near separation to help understand the features of the cracked surface.

Note that each row of Figure 3 is at a different global strain, in contrast to Figure 2. As can be seen in the figure, the cracked surface becomes rougher as loading rate increases. The global strain rate to achieve the configuration increases as well. The increase is also shown in the strain capacity chart in Figure 3. It is shown that the increase is approximately quadratic in the logarithmic scale. Also, density distribution shows a circular wave pattern centered at the crack tip. It implies the development of the shock wave near the crack tip at the boundary, and the feature becomes stronger at higher loading rates.

Figure 4 shows the temperature corresponding to snapshots of Figure 2. Although the external energy applied to each case is different, the change of ambient temperature is not observed except for the case of 5% of v_s where the failure mode is fundamentally different. In the first row, the temperature fluctuation is not obvious, while in the higher loading cases local heating is observed. The local heating becomes more obvious at higher loading rates, and appears at the crack tip. A closer look at the crack tip reveals that heating occurs in the head region of the crack tip and it explains the low density zone which shown in Figure 2. While energy is consumed, the potential energy is converted into kinetic energy (heat) and the converted energy is dissipated through heat transfer. An interesting feature that appears in the cases of 0.5 and 1.0% of v_s is the thermal fluctuation in the trailing region of the crack tip. This feature calls for a more detailed study of the failure mode under high loading rates. In the 5% of v_s case, heating shows a complicated pattern. However, one consistent feature is observed, that, divided by the inclined crack surfaces, the left and right boundary regions show heating while the material is relatively cool near the upper boundary and the lower boundary region is heated around the notch.

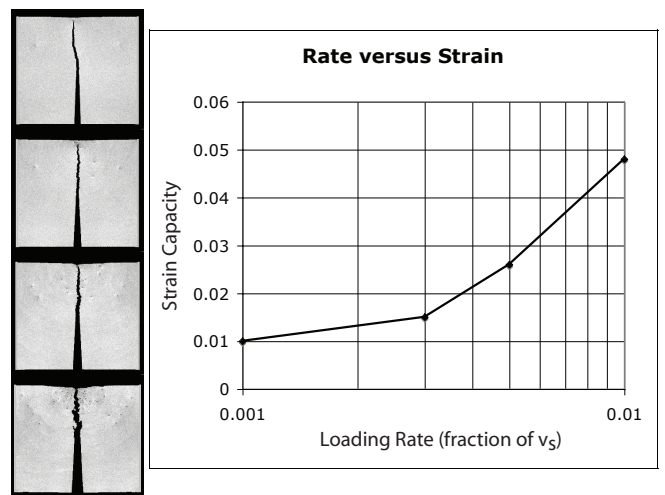


Figure 3. Crack propagation profile represented in density variation. Specimens corresponding to near separation configurations (From the top, loading rates are 0.1%, 0.3%, 0.5%, 1.0%, and 5.0% of v_s). Global strain at each row is 1.0%, 1.5%, 2.6%, and 4.8%.

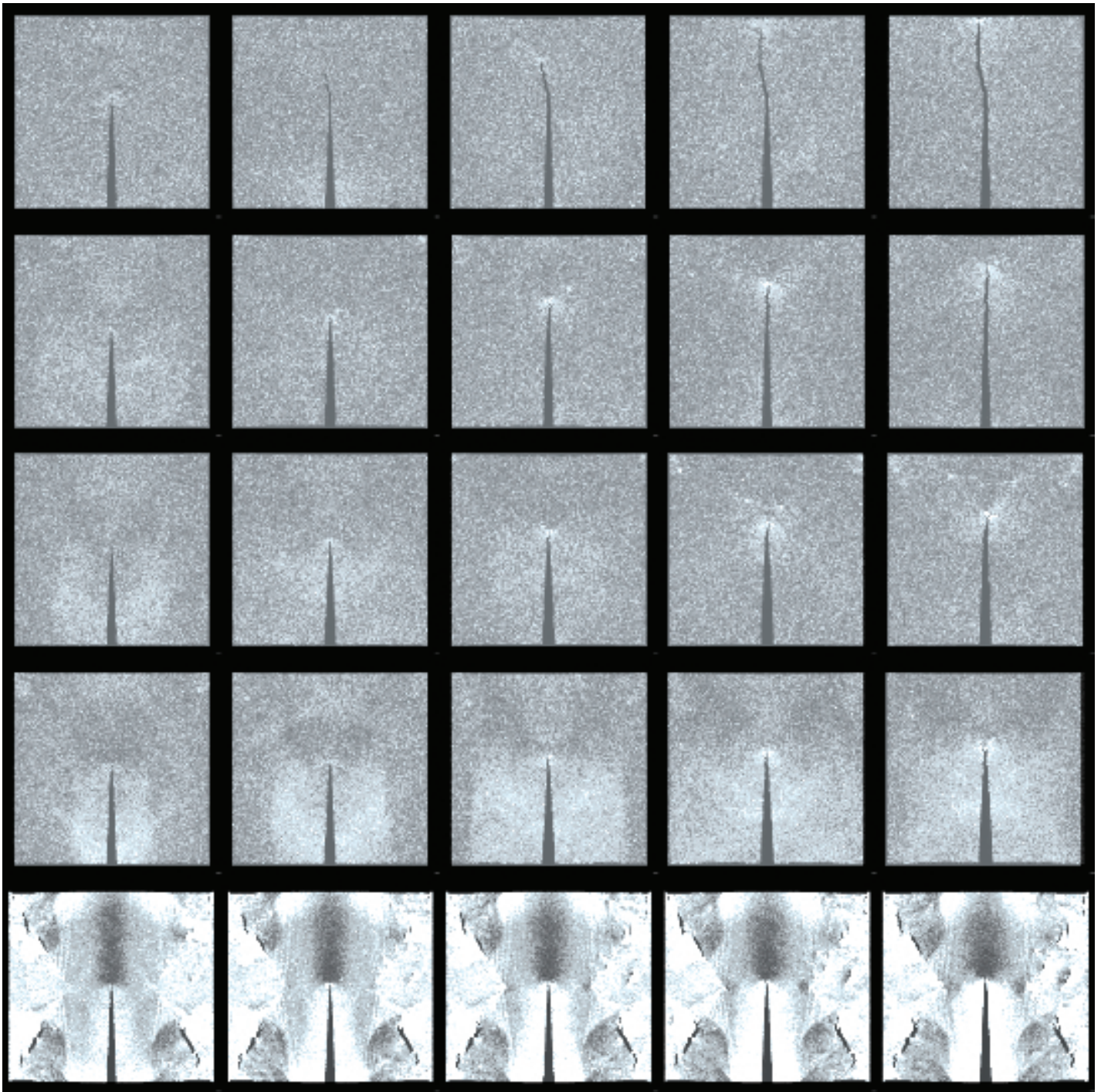


Figure 4. Crack propagation profile represented in temperature variation. Specimens corresponding to 5 different loading rates (0.1%, 0.3%, 0.5%, 1.0%, and 5.0% of v_s) are arranged in rows, and each column depicts a snapshot at the same global strain (0.15%, 0.3425%, 0.535%, 0.7275%, and 0.92%). Brightness of the figure is byte scaled to 0–30% of melting point.

For a detailed view, Figure 5 shows magnified snapshots around the crack tips during crack propagation. Strain at each case is chosen to be $2/3$ of the strain used in Figure 3. There are several features that can be observed:

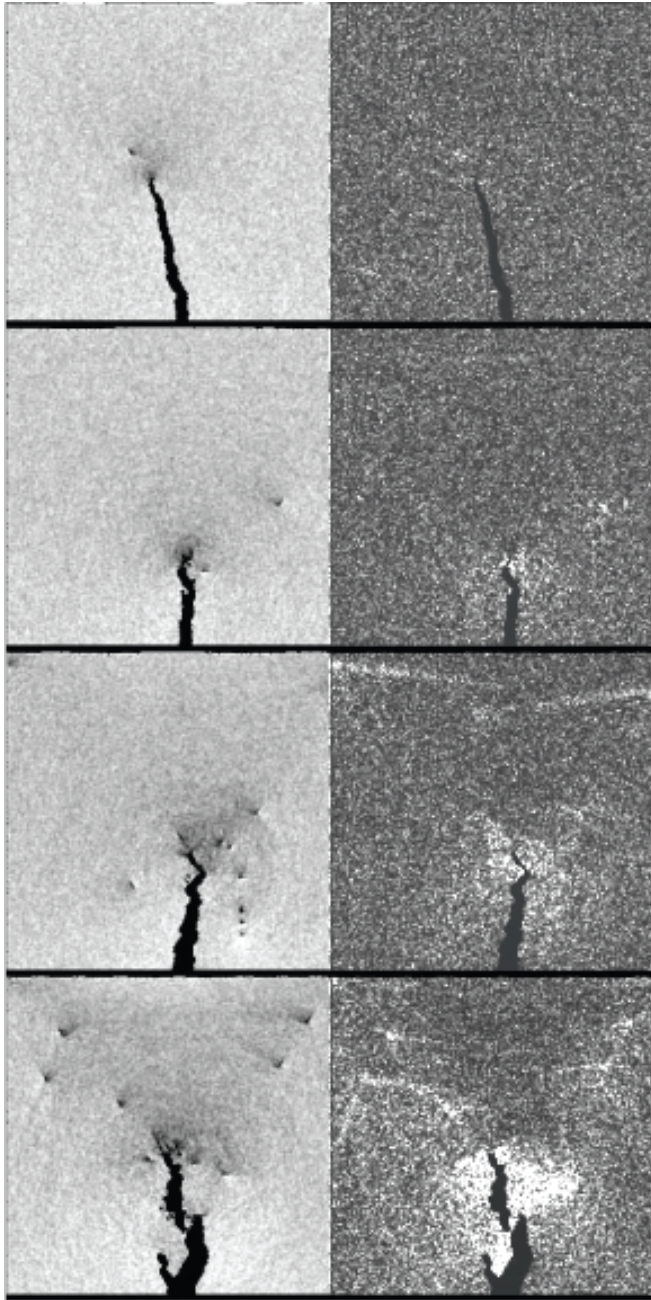


Figure 5. Magnified crack tip corresponding to global strain of 0.33%, 0.50%, 0.86%, and 1.6% from the top (loading rates are 0.1%, 0.3%, 0.5%, and 1.0% of v_s). Each snapshot shows the region of $x \in (185, 415)$ and $y \in (335, 565)$. Left column shows density distribution and right column shows temperature distribution.

- A shockwave is developed at the crack tip at higher loading rates. The circular wave pattern becomes more pronounced as the loading rate increases. Where the feature is distinct (3rd and 4th rows), bubble-like flaws are generated along the wave path. The flaws are seen to be traveling with the shockwave.
- Crack propagation shows jumps in the case of the highest loading rate (4th row). Instead of the crack developing continuously, an isolated crack is developed in the low density zone ahead of the crack tip. Then the isolated crack grows to connect with the following crack.
- Local heating at the crack tip becomes more evident at higher loading rates. Also, the heating is located ahead of the tip in the cases of row 1, 2, and 3, while in the last row heating is placed behind the tip. This may imply that the isolated crack is in the heated region of the following crack, and the generation of the isolated crack is motivated by combined heating and density lowering in the region.
- Location of low density and high temperature regions do not necessarily coincide. This feature may imply that the time of material softening and thermal heating are not synchronized.

4 CONCLUSIONS

A *numerical experiment* of the tensile notch test is performed and the results are presented. The results strongly imply that the fracture behavior of LJ material at high loading rate might change significantly when compared to the static cases. The main features observed from the analysis as loading rate increases are:

- Retardation of crack propagation speed
- Local heating around the crack tip
- Generation of shockwave at the crack tip
- Change of crack growth mode
- Roughening of cracked surface
- Higher strain capacity demand for crack growth
- Change of failure mode

Although the results presented in this study give a qualitative understanding of crack propagation, the data deserve further analysis in the following direction:

- Measurement of local stress and strain. Due to the complexity of stress-strain analysis at high strain rate, only global strain is measured and used as a parameter in this study. Local stress measurement is also omitted since corresponding local strain is not measured. To fully grasp the picture of dynamic cracking, the stress-strain relationship should be measured at several sampling points. The measurement may be especially important in analyzing the process of the material dominant failure mode shown in the 5% of v_s case shown in Figure 2 and 4.
- Measurement of toughness and fracture energy. Once the quantities are available, the model can be used to quantify the change of material properties from the static case, where a conventional analysis and experiment can provide the static data.
- A method to sustain desired strain rates. The material used in the study is nonlinear and strain rate is present locally. However, the value of the strain rate varies spatially and fluctuates through time. A method to fix the strain rate locally is needed so that measurements can be related to the strain rate. Material properties are reported to vary according to strain rate in various researches. The method presented in this study may be modified to give results in terms of more conventional strain rate, instead of loading rate.

Wagner, N. J., Holian, B. L., & Voter, A. F. 1992. Molecular-dynamics simulation of two-dimensional materials at high strain rates. *Physical Review A* 45(12): 8457–8470.

The above mentioned directions can be considered as quantitative studies. Future research is, thus, reserved for quantifying the material properties identified by the qualitative features observed in this study.

REFERENCES

- Buehler, M. J., Abraham, F. F., & Gao, H. 2003. Hyperelasticity governs dynamic fracture at a critical length scale. *Nature* 426(13): 141–146.
- Buehler, M. J. & Gao, H. 2006. Dynamical fracture instabilities due to local hyperelasticity at crack tips. *Nature* 439: 307–310.
- Gao, H., Huang, Y., & Abraham, F. F. 2001. Continuum and atomistic studies of intersonic crack propagation. *Journal of Mechanics and Physics of Solids* 49: 2113–2132.
- John, R. & Shah, S. 1990. Mixed-mode fracture of concrete subjected to impact loading. *Journal of Structural Engineering* 116(3): 585–602.
- Krivtsov, A. M. & Wiercigroch, M. 2001. Molecular dynamics simulation of mechanical properties for polycrystal materials. *Materials Physics and Mechanics* 3: 45–51.
- Lok, T. S., Zhao, P. J., & Lu, G. 2003. Using the split hopkinson pressure bar to investigate the dynamic behaviour of sfrc. *Magazine of Concrete Research* 55(2): 183–191.